Patterns

ADSeg: A flap-attention-based deep learning approach for aortic dissection segmentation

Highlights

- A novel flap attention module is proposed for segmenting type B aortic dissection
- A cascaded network structure with feature reuse and a two-step strategy is presented
- Evaluation was performed on a multicenter dataset including with or without thrombus
- The proposed method outperforms previous state-of-the-art deep learning methods

Authors

Dongqiao Xiang, Jiyang Qi, Yiqing Wen, ..., Huangxuan Zhao, Xinggang Wang, Chuansheng Zheng

Correspondence

fyang@hust.edu.cn (F.Y.), zhao_huangxuan@sina.com (H.Z.), xgwang@hust.edu.cn (X.W.), hqzcsxh@sina.com (C.Z.)

In brief

The post-processing of computed tomography angiography (CTA) images of an aortic dissection is a time-consuming and laborious process that requires extensive manual refinement, which can delay urgent clinical decisions. More automated methods have recently been developed to segment the true and false lumen of an AD, but they are limited in accuracy and performance. Herein, we propose ADSeg, a module that utilizes deep learning and is based on the flap attention mechanism, which is able to accurately segment the dissection lumen regardless of the dissection state. The effectiveness and generalizability of our model have been validated with a multicenter dataset.

Xiang et al., 2023, Patterns *4*, 100727
May 12, 2023
https://doi.org/10.1016/j.patter.2023.100727

Patterns

CellPress
OPEN ACCESS

Article

ADSeg: A flap-attention-based deep learning approach for aortic dissection segmentation

Dongqiao Xiang,[1,2,8] Jiyang Qi,[3,8] Yiqing Wen,[3,8] Hui Zhao,[4,8] Xiaolin Zhang,[5] Jia Qin,[5] Xiaomeng Ma,[6] Yaguang Ren,[7] Hongyao Hu,[4] Wenyu Liu,[3] Fan Yang,[1,2,*] Huangxuan Zhao,[1,2,*] Xinggang Wang,[3,*] and Chuansheng Zheng[1,2,9,*]

[1]Department of Radiology, Union Hospital, Tongji Medical College, Huazhong University of Science and Technology, Wuhan 430022, China
[2]Hubei Province Key Laboratory of Molecular Imaging, Wuhan 430022, China
[3]School of Electronic Information and Communications, Huazhong University of Science and Technology, Wuhan 430074, China
[4]Department of Interventional Radiology, Renmin Hospital of Wuhan University, Wuhan 430060, China
[5]Department of Radiology, Yichang Central People's Hospital, Yichang 443003, China
[6]Department of Radiology, Jingzhou First People's Hospital of Hubei province, Jingzhou 434000, China
[7]Research Laboratory for Biomedical Optics and Molecular Imaging, Shenzhen Institutes of Advanced Technology, Chinese Academy of Sciences, Shenzhen 518055, China
[8]These authors contributed equally
[9]Lead contact
*Correspondence: fyang@hust.edu.cn (F.Y.), zhao_huangxuan@sina.com (H.Z.), xgwang@hust.edu.cn (X.W.), hqzcsxh@sina.com (C.Z.)
https://doi.org/10.1016/j.patter.2023.100727

THE BIGGER PICTURE An aortic dissection (AD) is a serious condition in which the inner layer of the aorta tears, causing the inner and middle tissue layers to split as blood surges through the tear. Image processing to segment and visualize the anatomy of an AD is essential for disease diagnosis, surgical planning, and postoperative follow-up. In this study, we propose a deep learning method to improve the accuracy of image processing when segmenting the true and false lumen of an AD. When compared with the current optimal methods, our method more accurately discerns the anatomic features of AD, which may increase the likelihood for successful surgery and reduction of postoperative complications. Our overarching goal is to develop an intelligent platform for accurate diagnosis of AD, individualized surgical planning, and prognosis prediction, which will improve the survival of patients with AD. Given the high mortality rate of AD, any improvement in diagnosis and treatment efficiency could have substantial benefits for the healthcare system and patient well-being.

1 2 3 4 5 **Proof-of-Concept:** Data science output has been formulated, implemented, and tested for one domain/problem

SUMMARY

Accurate and rapid segmentation of the lumen in an aortic dissection (AD) is an important prerequisite for risk evaluation and medical planning for patients with this serious condition. Although some recent studies have pioneered technical advances for the challenging AD segmentation task, they generally neglect the intimal flap structure that separates the true and false lumens. Identification and segmentation of the intimal flap may simplify AD segmentation, and the incorporation of long-distance z axis information interaction along the curved aorta may improve segmentation accuracy. This study proposes a flap attention module that focuses on key flap voxels and performs operations with long-distance attention. In addition, a pragmatic cascaded network structure with feature reuse and a two-step training strategy are presented to fully exploit network representation power. The proposed ADSeg method was evaluated on a multicenter dataset of 108 cases, with or without thrombus; ADSeg outperformed previous state-of-the-art methods by a significant margin and was robust against center variation.

INTRODUCTION

Aortic dissection (AD) is a life-threatening cardiovascular disease characterized by sudden onset, rapid progression, and high mortality.[1] A dissected aorta is often initiated on account of a tear in the aortic intima by which a surge of blood flows into the intima and media layers of the aortic wall, splitting the original single lumen of the aorta into the true lumen (TL) and false lumen (FL).[2] The thin intimal layer that separates the TL and FL is known as the intimal flap, which is a distinctive boundary between the TL and FL (Figure 1). Based on the segment involved in the dissection, the Stanford classification categorized AD into types A and B.[3] Type A AD involves the ascending aorta and requires urgent open surgery to replace the ascending aorta under direct vision. Type B AD involves only the descending aorta and is commonly treated with endovascular repair to implant a stent-graft to cover the intimal tear, which relies heavily on image guidance.[4,5] For untreated AD, mortality increases by 1%–2% per hour during the first 24 h, with reported mortality rates of 80% at 2 weeks.[1,6,7] For AD after treatment, close imaging follow-up is routinely required to detect possible severe postoperative complications in a timely manner.

Currently, computed tomography angiography (CTA) is the modality of choice for the diagnosis, risk evaluation, surgery/endovascular repair planning, and imaging follow-up of AD.[8] Based on the original CTA and reconstructed 3D images, the anatomic features of AD, including the extent of dissection, size and location of the tear, and diameter and geometrical morphology of the TL and FL, can be displayed intuitively and accurately. This is of great importance for surgeons in evaluating the risk of AD and making individualized surgical plans. Furthermore, thrombus formed by blood coagulation in the FL, which has been shown to be significantly associated with the prognosis of AD,[9] appears relatively hypodense on CTA images and is a challenging situation for TL and FL segmentation.[10] Aortic lumen segmentation is a necessary and difficult step in performing 3D visualization, accurate measurement, and creation of volumetric models for hemodynamic simulations.

Traditionally, commercial post-processing workstations for threshold-based segmentation and rendering have been semi-automatic and require extensive manual refinement by surgeons and radiologists. This process is complex and time-consuming, as the aortic CTA contains hundreds of slices, which may conflict with urgent clinical decisions. Accurate segmentation can be seen as a prerequisite step for perfect rendering. Because the blood flow in the FL is relatively slow and often accompanied by thrombus formation, threshold-based segmentation and rendering methods cannot effectively display a relatively low-density FL and thrombus. At the same time, the image reconstructed by this method is a 3D rendering of the entire aorta and cannot be saved as TL and FL segmentation maps. The 3D rendered images cannot be used for 3D visualization of lumens, hemodynamic simulation, and aortic diameter measurement.[11] Therefore, an efficient and automatic segmentation method is highly desirable.

Deep learning (DL) is a class of machine learning techniques that uses multilayered artificial neural networks for the automated analysis of signals or data. In recent years, convolutional neural networks (CNNs) have been widely used for medical image segmentation.[12–15] CNNs, composed of a convolution layer and nonlinear operator, are a high-performance embodiment of the DL technique. The CNN fits nonlinear equations using machine learning rather than manually providing equations for traditional image processing methods.[15] CNNs are very accurate in image recognition and classification and also minimize computation in comparison with a regular neural network. A few studies have attempted to automatically segment type B AD by using CNNs. Cao et al.[16] proposed a serial multi-task CNN model for automated segmentation of type B AD with the first network segmenting the entire aorta and the second network separating the TL and FL. Chen et al.[17] also followed this multi-stage learning framework and added an aorta straightening method between the two stages to alleviate the impact of the curved shape of the aorta and simplify the segmentation. Instead of using 3D modules, Hahn et al.[18] explored only 2D modules. They used the aortic lumen predicted by the first network to derive the multiplanar reformations (MPRs) orthogonal to the aortic centerline and input these MPRs into the second network to predict the final segmentation results. Lyu et al.[19] used both a 3D network for aorta partition and a 2D network for segmentation. They also applied an individual boundary detection network to extract boundary information. Furthermore, Wobben et al. developed three segmentation models using a 3D residual U-Net for the segmentation of TL, FL, and FL thrombosis.[20] Krissian et al. developed a semi-automatic segmentation tool based on a multi-step strategy to extract the AD wall and flap.[21]

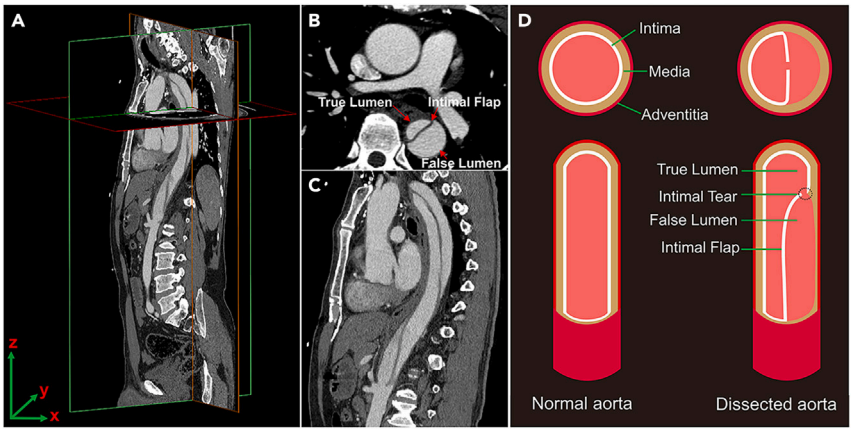

Figure 1. Schematic of aortic dissection

(A) Spatial distribution of aortic dissection in sagittal, transverse, and coronal planes on the CT image.

(B and C) The true lumen, false lumen, and intimal flap of aortic dissection in the axial (B) and sagittal slice (C).

(D) The cross-section and longitudinal-section views of the normal aorta and dissected aorta. The aortic wall is composed of intima, media, and adventitia. When the intima is torn, the intimal flap moves into the aortic lumen and separates it into the true and false lumens.

These methods have contributed to improving the segmentation accuracy of type B AD, but there have been some important limitations: (1) none of the above studies have regarded the segmentation of the characteristic intimal flap structure of AD as the guide of segmenting TL and FL. The intimal flap is a thin membranous structure between the TL and FL formed by tearing the intima of the arterial wall and is an anatomically clear dividing line between the TL and FL. Therefore, identification and segmentation of the intimal flap may be beneficial for more rapid and precise segmentation of the TL and FL. (2) Further, previous learning-based methods have depended only on the convolutional layers to aggregate the local Z-direction information. Considering that the aorta is typically approximately five times longer than the length of the x/y axis,[22,23] 3D local convolution layers may not be sufficient to capture the long-distance z axis information of the dissected aorta. It is very difficult to distinguish the TL and FL only by observing several adjacent slices; therefore, the interaction of long-distance Z-direction information across slices is necessary for the accurate segmentation of AD. (3) Although nearly all previous learning-based methods[16–19] used the cascaded network structure, limited by the multi-stage paradigm, none of them reused the features learned by the first network in the second one, which led to the strong representation power of the cascaded structure not being fully exploited. (4) From a data perspective, none of the previous studies have evaluated the multicenter performance of models trained with only one center, nor have they examined the respective performance of cases with and without thrombus. Therefore, the generalizability of these AD segmentation methods has not been effectively verified, potentially hindering clinical applications.

In this study, we aimed to develop a DL approach based on the flap attention module around the above four points and finally achieve accurate segmentation of the TL and FL. In summary, our main contributions are 3-fold.

(1) We propose a flap-attention-based AD segmentation method, termed ADSeg, which can automatically segment the TL, FL, and branch vessels (BR) of AD in an end-to-end manner. At the core of ADSeg is a flap attention mechanism that was specifically designed for the AD segmentation task. This mechanism can simplify the segmentation task and enhance the segmentation performance of the whole network by using key flap voxels with high confidence scores in the interface information predicted by the first network and integrating the long-distance z axis information and classifying the TL and FL from the upper and lower slicers over long distances (nearly 1,000 slicers per patient). We fully exploit the representation power of the cascaded network structure by further leveraging the obtained features of the first U-Net and adopting a two-step training strategy.

(2) We conduct extensive AD segmentation experiments with a multicenter dataset. Upon testing, ADSeg is found to outperform the previous methods by 5%–10%. Experiments further show that ADSeg trained with one-center cases can also perform well on cases from other centers, which demonstrates that our method has a strong generalizability and is robust to center variation. In addition, by evaluating the performance of the methods on cases with and without thrombus, we analyze the impact of thrombus and prove that ADSeg can improve AD segmentation performance, regardless of the presence of thrombus.

(3) Prior to this publication, there were no open-source datasets, so AD segmentation methods could not be directly compared. Here, we address this need by providing a high-performance codebase and a manually annotated multicenter dataset for the challenging AD segmentation task.

RESULTS

Study design

We proposed a flap-attention-based DL method, termed ADSeg, to segment the TL, FL, and BR of the dissected aorta. As shown in Figure 2, ADSeg takes a 3D CT volume as input and uses a two-step training strategy. After pre-processing, ADSeg uses two cascaded neural networks to extract the segmentation features, in which the first network is the classic U-Net[24] and the second is the proposed flap attention network (Figures 3 and 4), which are described in detail in the section on "flap attention." Each network is followed by a 3 × 3 × 3 convolution layer to generate the segmentation masks of the dissected aorta.

Comparison with previous methods

Given that no code of recent AD segmentation methods had been published, for a fair comparison, we re-implemented several existing methods[16,17,19] and compared their performance with that of ADSeg on our dataset. We provide the source code and trained models from the compared methods and our ADSeg method (https://doi.org/10.5281/zenodo.7703732). As shown in Table 1, by leveraging the specifically designed flap attention and two-step training strategy, ADSeg outperforms all existing methods by a large margin in terms of TL and FL segmentation. For example, compared with the previous top-performing method,[17] ADSeg results in improvements of 4.1% (91.1% vs. 87.0%) and 5.9% (88.4% vs. 82.5%) in the dice coefficient score of TL and FL, respectively, which demonstrates the effectiveness of ADSeg. The smaller standard deviation of ADSeg in TL and FL segmentation also indicates that ADSeg can generate more stable segmentation results for patients.

Among these methods, the results of Lyu et al.[19] are compromised because of the lack of Z-direction information. We also observe that the methods of Lyu et al. and Chen et al.[17] are significantly slower than other methods because of their complex and time-consuming aorta straightening strategies. By contrast, our proposed flap attention in ADSeg can naturally aggregate information along the curved shape of the aorta, which avoids the high time cost of the complex straightening method and endows ADSeg with the ability to be performed in an end-to-end manner.

Ablation study

To further prove the effectiveness of our proposed modules and strategies, we conducted exhaustive ablation experiments; the

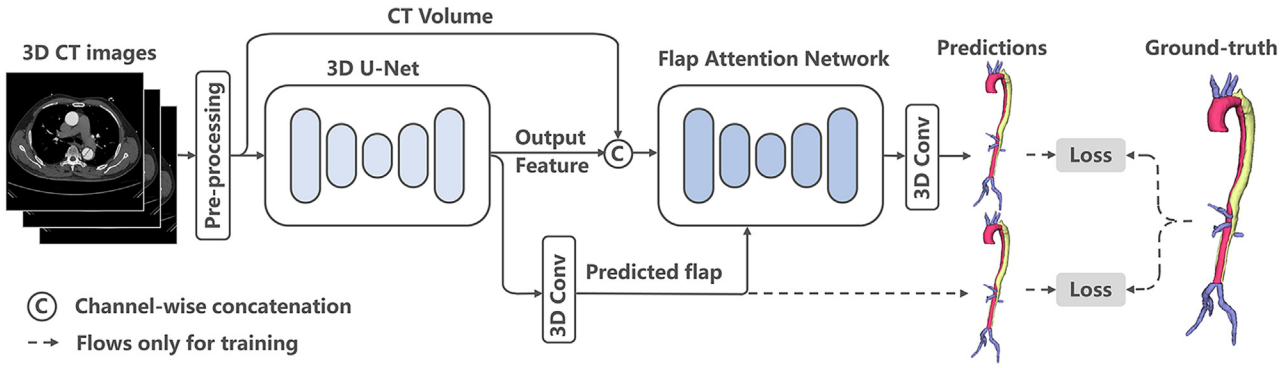

Figure 2. Overview of the proposed ADSeg

The network takes a CT volume as input and directly outputs the segmentation mask of a dissected aorta. It is mainly composed of two networks in which the first one is the classic U-Net and the second is further equipped with the specially designed flap attention module. More details regarding the network structure and flap attention module are shown in Figures 3 and 4 and the "overview of ADSeg" and "flap attention" sections. "Conv" denotes convolution layer.

results are presented in Table 2 and Figure 5. The first row in Table 2 shows the traditional 3D U-Net without any augmentation. The second row shows the two cascaded U-Nets with feature reuse but trained following the naive one-step training strategy. The third row shows the Cascaded U-Net+ mechanism trained using the two-step training strategy. Finally, the last row shows the proposed ADSeg, which further uses the flap attention mechanism.

As shown in Table 2, directly replacing a single 3D U-Net (first row) with two cascaded U-Nets (second row) without any adjustment to the training strategy can result in a large dice coefficient improvement of 3.2% (87.9% vs. 84.7%) for TL and 4.4% (85.4% vs. 81.0%) for FL. Moreover, when training with the two-step strategy (third row), the performance is further improved by 1.8% (89.7% vs. 87.9%) and 1.0% (86.4% vs. 85.4%) in terms of the TL and FL dice coefficients, respectively. We believe that the reason for these remarkable improvements is that with the two-step training strategy, the features learned by the first pre-trained U-Net significantly simplify the training of the second network. Based on the performance of the strong Cascaded U-Net+ mechanism, it can be concluded that adding flap attention modules (last row) further achieves a significant dice coefficient improvement of 1.4% (91.1% vs. 89.7%) for TL and 2.0% (88.4% vs. 86.4%) for FL. Benefiting from the two-step training strategy, the first pre-trained U-Net can also provide reliable flap predictions to the flap attention modules in the second flap attention network, which can stabilize and smooth the training of the network. The loss curves of the Cascaded U-Net with and without the two-step strategy are depicted in Figure 6.

In addition, as described in the section "flap attention," we predicted the flap voxels with the first network and selected the top-N voxels with the highest confidence score in each slice as the key voxels. For the smallest input feature, the number of key voxels per slice $N_{smallest}$ was set to one by default. A comparison of ADSeg using different key-voxel sampling strategies is presented in Table 3. If we use the random sampling strategy, the flap attention module does not improve the results, which demonstrates the importance of the newly designed sampling strategy with reference to flap predictions. In addition, sampling more key voxels results in no additional improvement, and only a small number of key voxels per slice is sufficient.

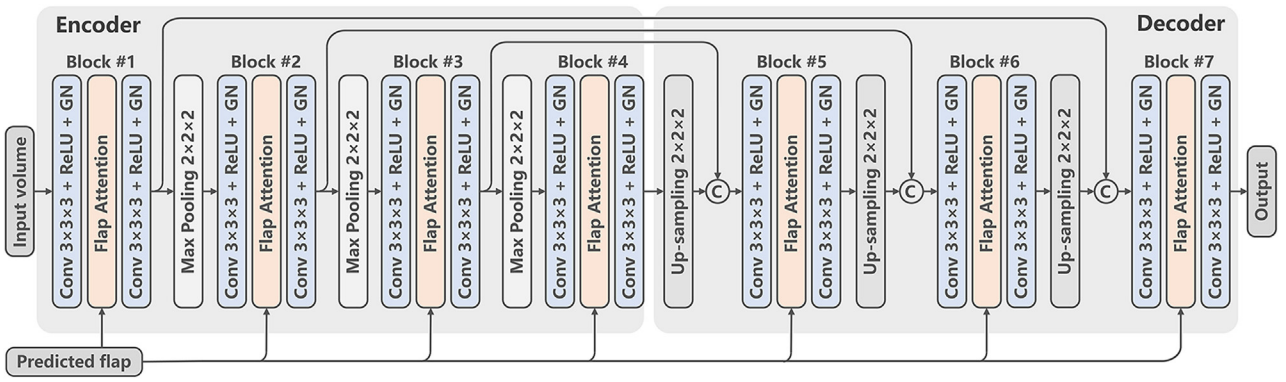

Figure 3. Structure of the flap attention network

The "predicted flap" is predicted by the first U-Net, and the "input volume" is the CT volume concatenated with the output feature of the first U-Net, as shown in Figure 2. Please refer to "overview of ADSeg" and Table 6 for more details about the network structure and Figure 4 and "flap attention" for details on the flap attention module. "Conv 3 × 3 × 3" denotes a convolutional layer with a kernel size of 3 × 3 × 3. "ReLU" represents rectified linear unit. "GN" means group normalization layer.

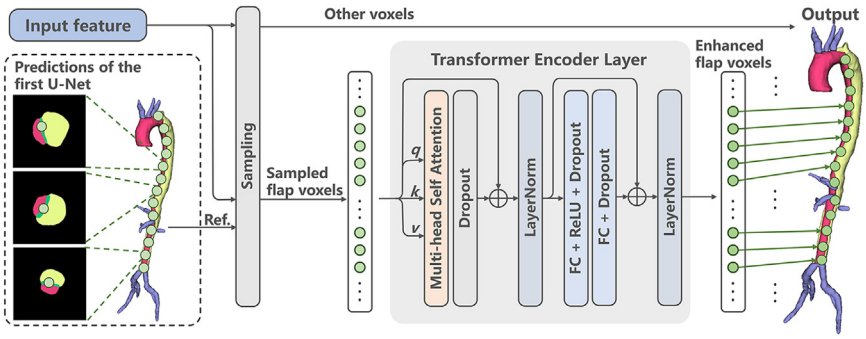

Figure 4. Pipeline of the flap attention module

As illustrated in flap attention, using the predictions of the first U-Net as references, we sample a set of key flap voxels and input them to the flap attention module. Subsequently, the sampled key flap voxels in the input feature are replaced by the enhanced voxels, while other voxels remain the same. The green regions in the 2D axial slices on the left are the flap segmentation results predicted by the first U-Net. The green points denote the *N* sampled key flap voxels per CT slice. "FC" represents fully connected layer. "ReLU" means rectified linear unit.

We also stacked more U-Nets, and no further gain was obtained regardless of whether the flap attention modules were added. This demonstrates that the capacity of the two cascaded U-Nets is sufficient for the AD segmentation task, and using three or more U-Nets will only slow down the inference speed with minor accuracy improvements.

Comparison with other attention mechanisms

We further demonstrate the effectiveness of the flap attention mechanism in elevating segmentation performance by comparing it with three other alternatives. The first option is traditional global pixel-wise attention, which is also known as the non-local operation.[25] The second option is to replace the flap attention with z axis attention, which only performs attention along the z axis. We also tested crisscross attention[26] as the third option, which exhibited excellent performance in general segmentation tasks. The computational complexity and AD segmentation performance of these three alternatives and the flap attention mechanism are presented in Table 4.

The dense attention operations of these three alternatives lead to extremely high complexity in both space and time. Limited by the high space complexity of 1 GPU with 16 GB memory, the global attention module can only be applied to the smallest feature map with stride $S = 8$, and the z axis attention and crisscross attention modules can only be applied to the feature maps with stride $S \geq 2$. By contrast, the computational complexity of the flap attention module is only $O(H2)$, which is significantly lower than those of the other three alternatives. This enables the flap attention module to be performed on all features in the network and capture finer information. The efficiency and performance gap between it and other alternatives increase remarkably with input resolution.

Moreover, although the flap attention mechanism requires negligible computational resources, it outperforms all other alternatives, especially in terms of the FL segmentation performance. Our interpretation is that the z axis and crisscross attention mechanisms struggle to handle the curved shape of the aorta. In addition, global attention cannot aggregate textural information that is limited by its high complexity. Further, they do not fully exploit the flap information. The flap attention mechanism focuses on the intimal flap and seamlessly performs information interaction along the curved aorta, which leads to its high performance.

Performance on cases with and without thrombus

Thrombus commonly exists in the FL of approximately 50% of patients with AD. To test the impact of thrombus and performance of ADSeg in handling thrombus, 40 cases in the entire test set were divided into two groups: (1) the first group contained 20 cases without any thrombus and (2) the second group contained 20 cases with thrombus. The performance of ADSeg on these two groups is shown in Table 5. As can be seen, ADSeg can achieve remarkable performance improvements in both groups, and the improvements in cases without thrombus are larger.

Performance on cases from different centers

As described in the "study patients" section, to verify the generalization ability and robustness of ADSeg and to prompt the application of automatic AD segmentation in the future, the cases in our test set were collected from four different centers with 10 cases per center. The results of ADSeg and several baselines are

Table 1. Comparison with previous AD segmentation methods

	Dice coefficient (%) ↑				Boundary distance (mm) ↓				FLOPs	Params	Time
Model	TL	FL	AO	BR	TL	FL	AO	BR	(G)	(M)	(s)
U-Net	84.7(7.6)	81.0(10.8)	92.7(2.6)	82.5(5.1)	1.83(1.6)	2.48(3.2)	1.07(0.9)	1.90(2.0)	1,000	4.08	0.20
Cao et al.[16,a]	85.4(7.2)	82.0(11.5)	92.7(3.2)	84.3(5.3)	1.72(1.2)	2.85(1.8)	1.55(1.3)	1.79(1.4)	1,932	8.02	0.38
Lyu et al.[19,a]	57.7(9.5)	62.8(13.3)	91.1(3.5)	72.8(7.2)	3.98(2.2)	4.67(4.0)	1.56(1.4)	2.01(1.6)	2,033	46.92	173.30
Chen et al.[17,a]	87.0(6.6)	82.5(8.0)	92.6(2.4)	78.5(6.1)	1.68(1.2)	2.74(1.7)	1.23(1.3)	1.73(1.4)	1,999	8.14	173.28
ADSeg (Proposed)	91.1(3.9)	88.4(6.2)	93.2(2.6)	84.9(7.0)	1.47(0.8)	2.10(1.3)	1.06(0.6)	1.80(2.2)	2,194	8.29	0.53

↑ indicates the larger the better and ↓ indicates the smaller the better.

[a]epresents re-implementation of the methods. The standard deviations are also reported in brackets.

Table 2. Ablation study of ADSeg

Model	Cascaded	Two-step	Flap attn.	Dice coefficient (%) ↑				Boundary distance (mm) ↓				FLOPs (G)	Params (M)	Time (s)
				TL	FL	AO	BR	TL	FL	AO	BR			
U-Net				84.7(7.6)	81.0(10.8)	92.7(2.6)	82.5(5.1)	1.83(1.6)	2.48(3.2)	1.07(0.9)	1.90(2.0)	1,000	4.08	0.20
U-Net with flap attn.			√	87.6(5.4)	84.9(8.8)	92.6(3.2)	82.2(5.0)	1.64(1.2)	2.35(1.7)	1.05(0.7)	1.96(1.0)	20000	8.25	0.52
Cascaded U-Net	√			87.9(5.6)	85.4(7.4)	92.4(2.6)	80.2(5.3)	1.65(1.0)	2.54(2.8)	1.04(0.6)	2.29(1.7)	2,194	8.20	0.46
Cascaded U-Net+	√	√		89.7(4.9)	86.4(8.0)	93.0(2.7)	84.9(6.8)	1.86(1.4)	2.50(2.5)	1.10(0.6)	1.76(2.1)	2,194	8.20	0.46
ADSeg (Proposed)	√	√	√	91.1(3.9)	88.4(6.2)	93.2(2.6)	84.9(7.0)	1.47(0.8)	2.10(1.3)	1.06(0.6)	1.80(2.2)	2,194	8.29	0.53

"Cascaded," "Two-step," and "Flap attn." denote the cascaded structure, two-step training strategy, and flap attention mechanism, respectively.

reported in Table 6. As can be seen, although the performances of different centers vary significantly, ADSeg constantly outperforms U-Net by a large margin of approximately 5%–10%.

Visualization of segmentation results

The testing results of the two cases are visualized in Figure 7 and shown in Video S1. As shown in the figure, compared with traditional U-Net, the segmentation results of ADSeg are clearly superior. Although Cascaded U-Net+ achieves similar segmentation results for the upper part of the aorta as ADSeg, its segmentation results for the lower part of the aorta are usually unsatisfactory. By contrast, benefiting from the long-distance z axis attention along the intimal flap, ADSeg generates accurate segmentation results for the entire aorta.

The detailed segmentation results for six other cases, with and without thrombus, are shown in Figure 8. We can observe that by paying more attention to the intimal flap, ADSeg can better perceive the flap and accurately separate the TL and FL. Even for challenging cases with partial and complete thrombosis in the FL, ADSeg can recognize the coagulated FL by aggregating information from other slices along the aorta.

Quantitative analysis of lumen volumes

Furthermore, we calculated the volumes of the segmented TL and FL to evaluate the segmentation accuracy. TL and FL volumes were among the most important morphological characteristics for individual surgical planning and prognostic assessment. The U-Net, Cascaded U-Net, Cascaded U-Net+, and proposed ADSeg strategies were all compared with manual quantification using Bland-Altman analysis, and the results are shown in Figure 9. The Bland-Altman analysis results show that TL and FL volumes segmented using the proposed ADSeg are more consistent with manual segmentation.

Comparison between single-center and multicenter training sets

In order to observe the effect of using single-center training set and multicenter training set on the training results, we tried to train our proposed network using a multicenter training set. Specifically, the single-center training set is the same as shown in the text. The multicenter training set is also 68 cases, which is composed of four centers, with 53 cases in center 1 and 5 cases in each of centers 2 to 4. The test set consists of 20 cases, 5 cases in each center. As shown in the Table 7, the networks trained on the new multicenter training set performed slightly worse than those trained on the original single-center training set. This may be due to the small amount of data in centers 2 to 4, which leads to data imbalance of the multicenter training set. Larger and more balanced multicenter training data and additional test sets may help further improve the segmentation performance of the network.

DISCUSSION

In this study, we proposed a flap-aware AD segmentation framework called ADSeg and demonstrated its effectiveness. Given the CTA images of the dissected aorta, ADSeg automatically segments the TL, FL, BR, and intimal flaps in an end-to-end manner. At the core of ADSeg is the specifically designed flap attention mechanism that focuses on the intimal flap and leverages long-distance z axis information along the curved aorta. Furthermore, an optimized cascaded network structure with a two-step training strategy was developed to fully exploit the representation power of the networks. Upon comparing with other attention mechanisms and recent AD segmentation methods, the flap attention mechanism and ADSeg were found to be superior in terms of TL and FL segmentation.

As the core of ADSeg, the flap attention mechanism addresses three key points of AD segmentation simultaneously:

- *More attention is needed for the intimal flaps.* As illustrated above, intimal flaps require special attention for better separation of the TL and FL. The flap attention module is designed to address this problem by specifically enhancing the features of the flaps and enriching the semantics in those flap voxels.
- *Long-distance information interaction along z axis.* As the TL and FL can barely be distinguished by only observing several adjacent slices, the long-distance inter-slice interaction is of great importance for the accurate segmentation of the TL and FL, especially for slices far from the tear. Therefore, the flap attention module was designed to use a transformer encoder layer to implement communication among the flap voxels from different slices.
- *Feature extraction along the curved shape of the aorta.* By applying the transformer encoder layer only to flap voxels, the flap attention mechanism naturally performs feature

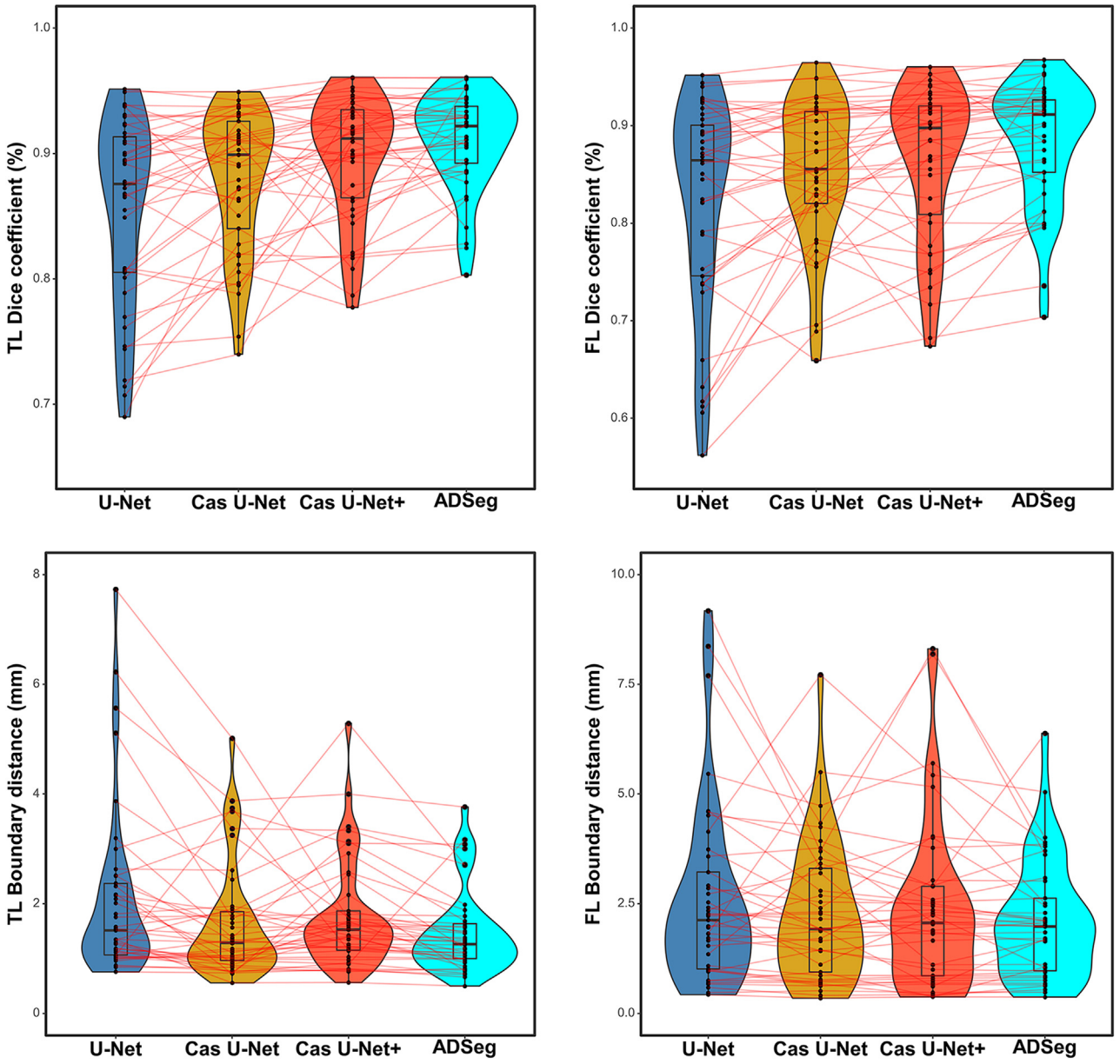

Figure 5. Violin plots of TL and FL dice coefficient and boundary distance of different strategies

In the middle of each density curve lies a small boxplot, with the rectangle showing the ends of the first and third quartiles and the central line showing the median. "Cas" denotes Cascaded.

interaction along the curved flap without the need for complex aorta straightening algorithms.[17,18] Moreover, the removal of these straightening operations also enables ADSeg to segment CT volumes in an end-to-end manner, instead of using the two networks individually, as in most recent works.[17–19] The resulting straightforward cascaded structure and newly proposed two-step training strategy can also boost the performance of ADSeg.

The two distinctive properties of the flap attention mechanism are (1) focusing on the key points (flap voxels in the AD segmentation task) and (2) incorporating long-distance interaction information. We believe that these two properties complement one another. As in the AD segmentation task, the enhancement of flap voxel features requires long-distance z axis information interaction. Correspondingly, long-distance z axis attention along the curved aorta must be performed on a set of key points along the aorta. Compared with other voxels in a slice, flap voxels are more important for accurate AD segmentation.

As shown in Tables 2 and 4, the specifically designed flap attention mechanism achieves significant performance improvement with respect to AD segmentation, especially for the segmentation of the FL and TL. In addition, leveraging the features

Table 3. Comparison between different sampling strategies of key voxels in the flap attention module

Sampling strategy	Dice coefficient (%) ↑		Boundary distance (mm) ↓	
	TL	FL	TL	FL
Random	90.0	86.6	1.62	2.48
$N_{smallest} = 1$	91.1	88.4	1.47	2.10
$N_{smallest} = 2$	90.9	88.4	1.52	2.03

"Random" setting indicates randomly sampling key voxels in the flap attention modules. $N_{smallest}$ denotes the number of key voxels per slice of the smallest feature map. "$N_{smallest} = 1$" setting is our default setting, and "$N_{smallest} = 2$" setting performs an additional sampling of the key voxels per slice.

obtained by the first U-Net and adopting the two-step training strategy led to complete exploitation of the representation power of the cascaded structure, greatly improving the segmentation performance.

In our experiments, to comprehensively test the performance of the methods, the test set we used consisted of cases from multiple centers with and without thrombus. As shown in Table 6, ADSeg trained with single-center data performs significantly well on cases from other centers. As shown in Table 5, ADSeg outperforms other baseline methods by a large margin, regardless of whether thrombus exists. These results demonstrate the strong generalizability and robustness of ADSeg. Moreover, we also observe (Table 5) that the TL segmentation performance on cases with thrombus is generally higher than that on cases without thrombus. By contrast, the FL segmentation performance on cases with thrombus is generally lower than that on cases without thrombus. This is because, with thrombus in the FL, the density of the FL decreases. The density difference between the TL and FL increases, making the boundary between the TL and FL clearer; however, the density difference between the FL and the surrounding tissue of the aorta decreases, making it difficult to distinguish the FL from the surrounding low-density tissue (e.g., fat).

Limitations and future directions

This study has several limitations, with several noteworthy issues that can be further studied. (1) Considering that ADSeg has shown significant improvement in the AD segmentation task, we believe that its network design and certain flap attention characteristics may be further improved by augmentation. This includes replacing the U-Net with more advanced basic networks such as PSPNet,[27] replacing the automatically generated flap annotations with human-annotated ground-truth data, or further adopting a "boundary attention" mechanism[28–30] that is similar to flap attention to improve the segmentation accuracy of aortic trunk (AO). (2) The AD segmentation performance of cases with thrombus should be further improved. Effectively distinguishing between thrombus and other surrounding tissues remains challenging for automatic AD segmentation tasks. (3) The prognosis[31] of AD, further leveraging these segmentation predictions, has not been explored in this study, which may have important theoretical and practical significance. (4) The main design philosophy of the flap attention mechanism, which focuses on the key component and performs feature interaction among a set of sampled unstructured key points, may also

Table 4. Comparison between flap attention and other attention mechanisms based on the Cascaded U-Net+

Attention mechanisms	Complexity	Dice coefficient (%) ↑		Boundary distance (mm) ↓	
		TL	FL	TL	FL
None	0	89.7	86.4	1.65	2.35
Global attention	$O(H^2W^2L^2)$	90.5	87.3	1.64	2.32
z axis attention	$O(H^2WL)$	90.3	87.6	1.74	2.63
Crisscross attention	$O(HWL(H+W+L))$	90.2	87.3	1.57	2.28
Flap attention (ours)	$O(H^2)$	91.1	88.4	1.47	2.10

"None" denotes the naive Cascaded U-Net+ without any attention modules. H, W, and L denote the length of the z, x, and y axes, respectively.

Table 5. Comparison on cases with and without thrombus

Group	Model	Dice coefficient (%) ↑		Boundary distance (mm) ↓	
		TL	FL	TL	FL
Without thrombus	U-Net	82.4	83.4	2.09	3.48
	Cas U-Net	87.0	87.6	1.72	1.90
	Cas U-Net+	88.9	89.1	2.18	1.64
	ADSeg	90.1	90.2	1.60	1.83
With thrombus	U-Net	87.0	78.5	1.56	4.96
	Cas U-Net	88.8	83.2	1.59	3.18
	Cas U-Net+	90.6	83.8	1.56	3.36
	ADSeg	92.0	86.6	1.34	2.38

"Cas" denotes Cascaded.

Table 6. Comparison on cases from different centers

Center	Model	Dice coefficient (%) ↑		Boundary distance (mm) ↓	
		TL	FL	TL	FL
# 1	U-Net	81.5	80.2	3.06	2.67
	Cas U-Net	85.1	84.9	2.30	1.96
	Cas U-Net+	87.5	87.1	2.37	2.12
	ADSeg	89.8	89.6	2.04	1.78
# 2	U-Net	89.1	82.2	1.56	2.21
	Cas U-Net	90.4	84.4	1.41	3.94
	Cas U-Net+	91.7	85.4	1.26	2.71
	ADSeg	91.8	86.7	1.40	2.20
# 3	U-Net	85.8	85.3	1.40	1.59
	Cas U-Net	88.5	88.4	1.21	1.28
	Cas U-Net+	91.0	89.7	1.44	1.35
	ADSeg	91.9	90.6	1.04	1.38
# 4	U-Net	82.4	76.1	2.63	4.94
	Cas U-Net	87.5	83.9	1.69	2.97
	Cas U-Net+	88.8	83.6	2.40	3.85
	ADSeg	90.7	86.7	1.40	3.07

"Cas" denotes Cascaded.

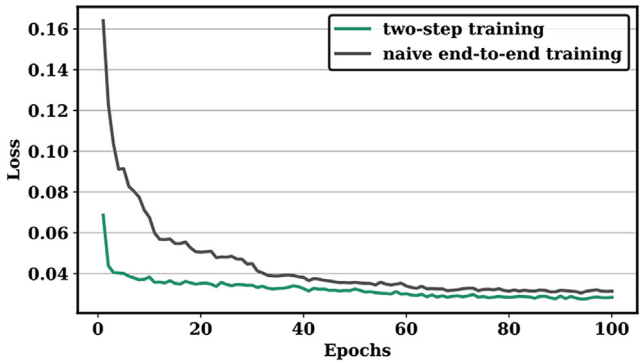

Figure 6. Loss curves of Cascaded U-Net trained with the naive end-to-end training strategy and Cascaded U-Net+ trained with the two-step training strategy.

benefit other related segmentation tasks (e.g., vascular segmentation,[30,32–34] and cell boundary segmentation[35]). Further exploration of the application of this design philosophy in other segmentation tasks may be meaningful.

Conclusions

In conclusion, we explored the effect of leveraging flap information and long-distance z axis information interactions on AD segmentation. Benefiting from the specifically designed flap attention module and optimized cascaded network structure, our proposed ADSeg achieves higher performance than other AD segmentation methods and our baselines and demonstrates strong generalizability on a complex multicenter test set. Therefore, we believe that ADSeg has great potential to be deployed in clinical applications to assist in the diagnosis and individualized treatment of AD.

EXPERIMENTAL PROCEDURES

Resource availability

Lead contact

Chuansheng Zheng, hqzcsxh@sina.com.

Materials availability

This study did not generate new unique reagents.

Data and code availability

All of the original code and a manually annotated multicenter dataset with three centers have been deposited at Zenodo under the https://doi.org/10.5281/zenodo.7703732, which is publicly available as of the date of publication. All publicly available data were anonymized, including the removal of patient information, center names, and scan parameters. One center's data were not approved for public release. Any additional information required to reanalyze the data reported in this paper is available from the lead contact upon request.

Methods

Study patients

The multicenter dataset of this study was retrospectively collected from four centers: the Union Hospital of Huazhong University of Science and Technology,

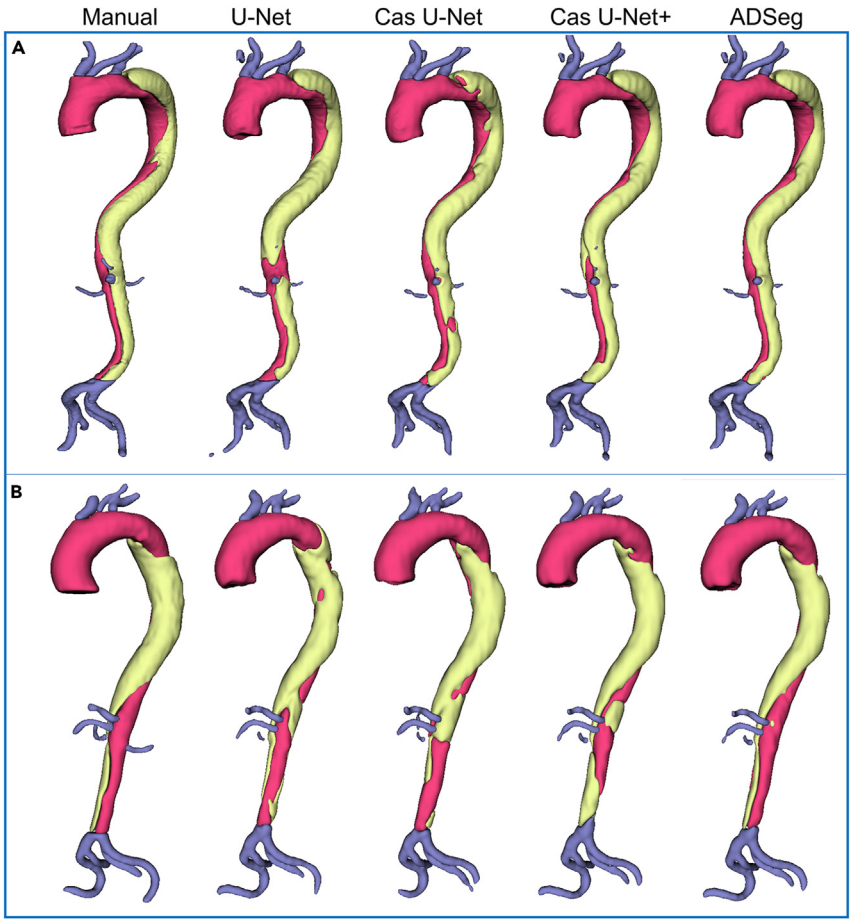

Figure 7. 3D visualization of segmentation results

(A and B) Based on different strategies, (A) and (B) show aortas without and with thrombus in the false lumen, respectively. "Cas" denotes cascaded.

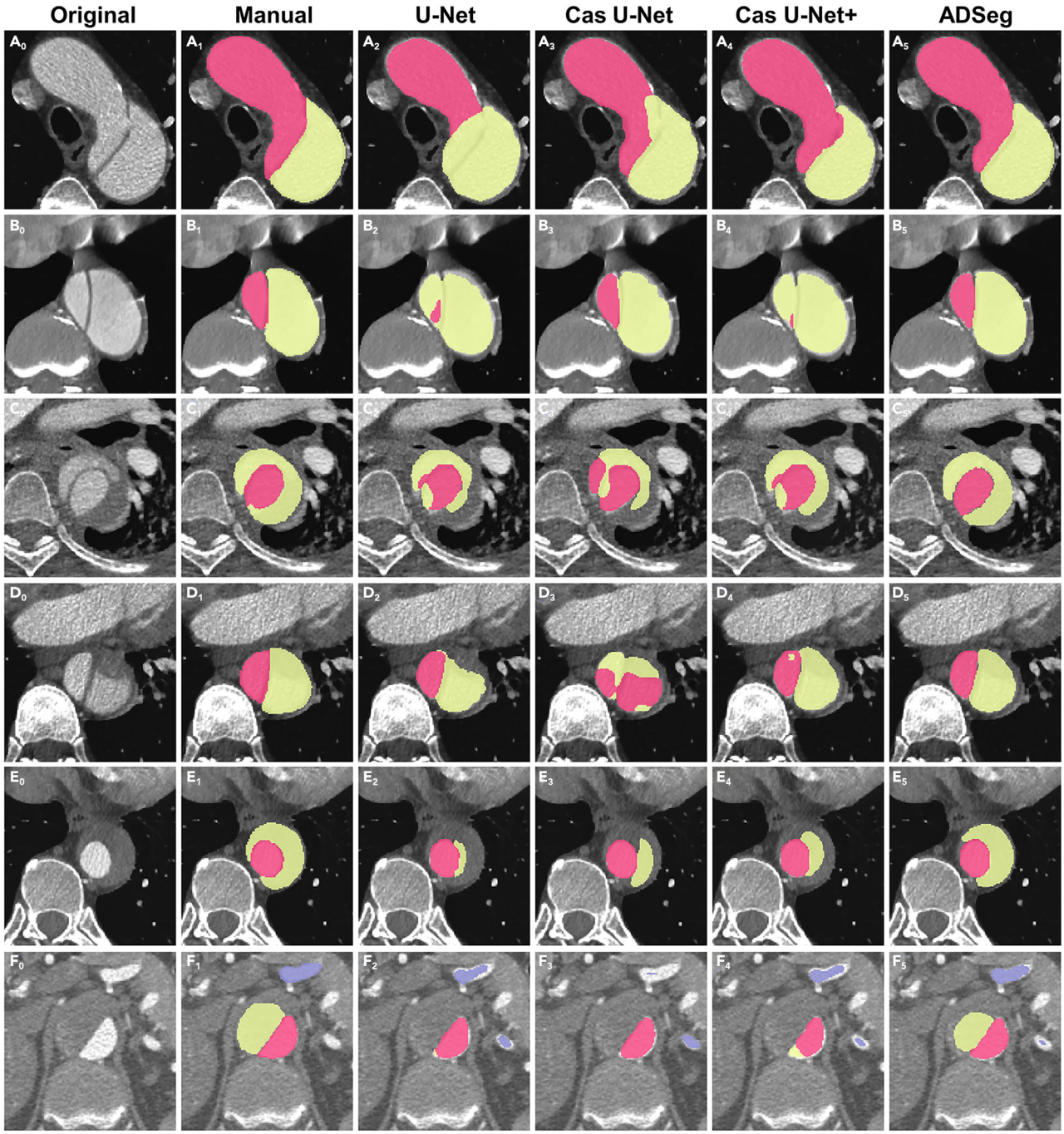

Figure 8. Segmentation details based on different strategies in patients with and without thrombus in the FL

The red areas represent the TL, and the yellow areas represent the FL. $A_{0\text{-}5}$ and $B_{0\text{-}5}$ show the cases with patent FL. $C_{0\text{-}5}$ and $D_{0\text{-}5}$ show the cases with partial FL thrombosis. $E_{0\text{-}5}$ and $F_{0\text{-}5}$ show the cases with complete FL thrombosis. "Cas" denotes cascaded.

Renmin Hospital of Wuhan University, Yichang Central People's Hospital, and Jingzhou First People's Hospital. A total of 108 patients (mean age: 57.8 ± 12.9 years; 93 males) diagnosed with Stanford type B AD according to aortic CTA between January 2010 and December 2020 were included in this study. Data from 68 patients from the Union Hospital of the Huazhong University of Science and Technology were used to train the proposed ADSeg framework. Among the 68 patients in the training set, 35 (51.5%) had different degrees of thrombosis in the FL. No thrombosis was observed in 33 (48.5%) patients. Data from an additional 40 patients (10 cases per center) from the four centers were used for internal and external testing, including 20 cases with and 20 cases without thrombosis. All CTA data were obtained preoperatively, and the patients did not receive surgery/endovascular interventions. The protocol of this multicenter study was approved by our institutional review board, and the local institutional review board of each center approved the use of the CTA data. Written informed consent was waived due to the retrospective nature of the enrolled cohort.

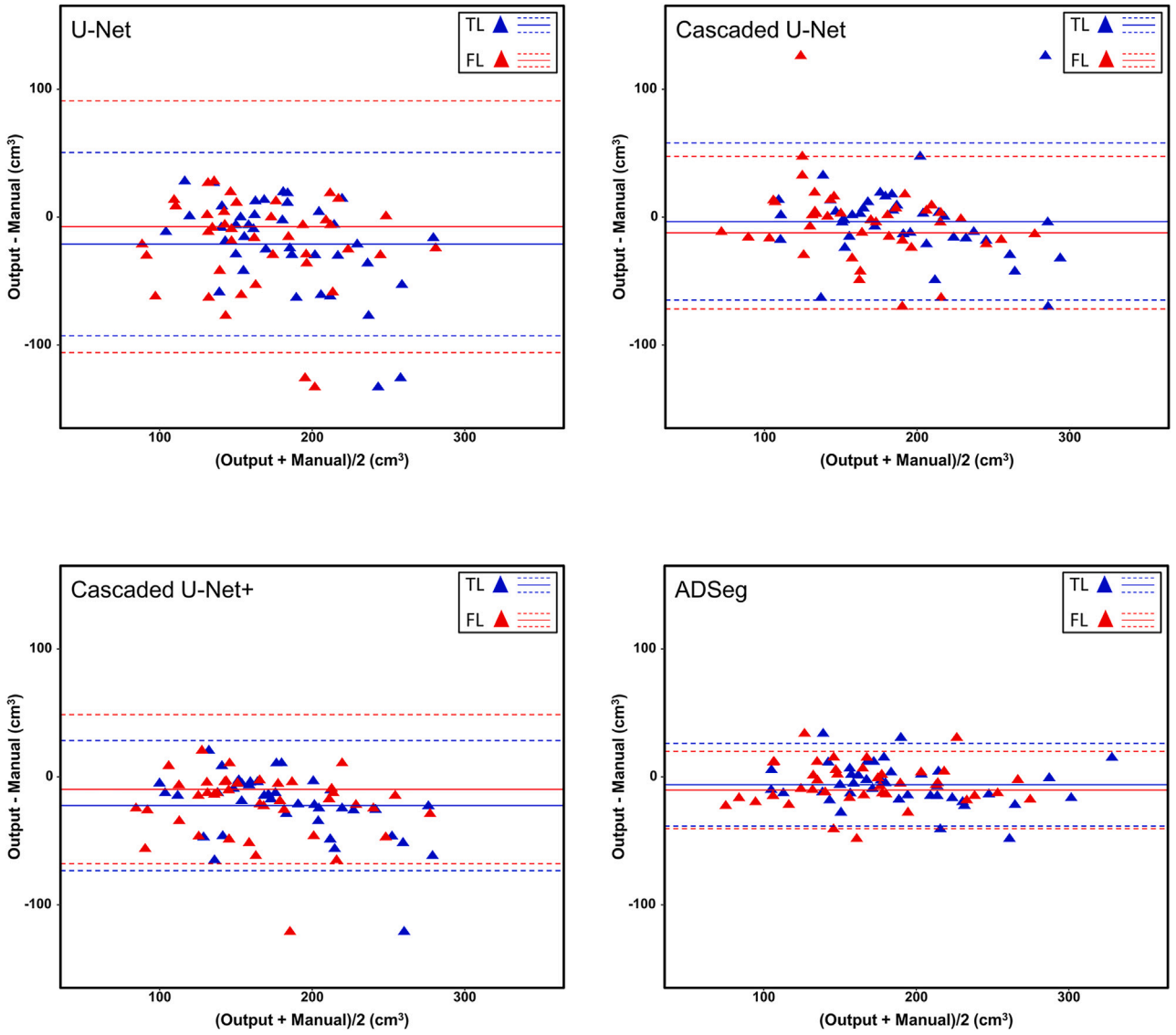

Figure 9. Bland-Altman analysis of the TL and FL volumes of U-Net, Cascaded U-Net, Cascaded U-Net+, and proposed ADSeg strategies
The solid line represents the mean value of the difference from the manual, and the dashed line represents the 95% confidence interval of the difference.

Image acquisition

CTA scanning was performed with various multidetector row spiral CT devices, including the Discovery CT750 HD (GE Healthcare), Revolution CT (GE Healthcare), SOMATOM Definition AS (Siemens Healthineers), SOMATOM Definition Flash (Siemens Healthineers), Optima CT680 Series (GE Healthcare), and Philips Ingenuity CT (Philips Healthcare). A tube voltage of 100–120 kV was used for all patients, and the tube current ranged from 116 mA to 656 mA. Aortic CTA scanning was performed from the level of the thoracic inlet to the pelvic floor after the injection of intravenous contrast material. The other relevant parameters are as follows: pixel spacing, 0.49–0.90 mm; reconstruction slice thickness, 0.625–1.25 mm; matrix, 512 × 512. The total number of CTA slices was 106,426 in all patients, with an average of 985 ± 299.5.

Ground-truth label

All 108 CTA datasets were manually segmented by an experienced radiologist (D.X., with 10 years of experience in cardiovascular imaging) using the medical image processing software Mimics 21.0 (Materialise, Leuven, Belgium). Every dataset was labeled slice by slice in axial view into TL, FL, BR, and background, and the entire aorta was the integration of TL and FL. If a thrombus was present in the FL, it was included and labeled FL. BR consisted of the brachiocephalic artery, left common carotid artery, left subclavian artery, celiac trunk, superior mesenteric artery, double renal arteries, and iliac artery. The endpoints of the BR were generally set at the first bifurcation of the branch trunk according to the anatomic characteristics, and the endpoints of the left common carotid artery and left subclavian artery were set at the same level as the brachiocephalic artery.

Table 7. Comparison of segmentation results between single-center training set and multicenter training set

	Dice coefficient (%) ↑		Boundary distance (mm) ↓	
Training set	TL	FL	TL	FL
Single-center training set	91.2	90.7	1.60	1.86
Multicenter training set	90.4	90.0	1.68	1.96

Table 8. Feature resolution and number of channels in ADSeg

Block		C_{input}	C_{inner}	C_{output}	Resolution
Encoder	Block #1	1 (65)	32 (65)	64	240 × 96 × 96
	Block #2	64	64	128	120 × 48 ×48
	Block #3	128	128	256	60 × 24 × 24
	Block #4	256	256	512	30 × 12 × 12
Decoder	Block #5	1024	256	256	60 × 24 × 24
	Block #6	512	128	128	120 × 48 × 48
	Block #7	256	64	64	240 × 96 × 96

C_{input} and C_{output} denote the input and output channel numbers of the block, respectively. C_{inner} denotes the output channel number of the first convolution layer, which is also equal to the input channel number of the second convolution and channel number of the optional flap attention module. The numbers in the "Resolution" column are in the order of "z axis length (number of slices) × x axis length × y axis length." Most numbers shown in the table are the same for the first and second networks. We report the values of the second network in brackets if they differ from that of the first U-Net.

The specific annotation process was briefly summarized as follows: first, the CTA images were imported in Digital Imaging and Communications in Medicine (DICOM) format, the window width was set to 700 HU and window level to −150 HU, a new mask was created, the threshold was adjusted to 175 to 600 HU, and holes were checked; second, the Crop Mask tool was used to narrow the volume of interest down, and the Split Mask tool was then used to separate the aorta from other tissues; third, the Edit Mask tool was used to erase a slice at the initiation site of BR, and the Split Mask tool was used to segment the whole aorta and BR; finally, the Split Mask tool was used to separate the TL and FL with the intimal flap as a boundary, and the thrombus that could not be identified by the above threshold was manually annotated. Manual annotation took approximately 2–3 h per dataset depending on the extent of thrombosis.

Experimental details

The ADSeg software was developed based on the PyTorch framework[36] using an NVIDIA GeForce GTX 2080Ti GPU. The number of groups in group normalization and number of heads in the multi-head self-attention module were eight each. The dropout probability for all dropout layers in the flap attention modules was 0.1. For both training steps, the networks were trained for 50 epochs using the Adam optimizer[37] with an initial learning rate of 5e-4 and a weight decay of 2e-4. The batch size was set to 1. Softmax and dice loss functions were used to calculate the losses between the predictions and ground-truth labels of the background, TL, FL, and BR. It is worth noting that as the generated flap category is not exclusive to other categories (e.g., background, TL, and FL), the losses of flap predictions should be calculated individually with the sigmoid and dice loss functions. The loss weights for the TL, FL, BR, and flap were 0.3, 0.3, 0.3, and 0.1, respectively.

For the dataset, we split the 108 cases into two sub-sets: (1) the development split with 68 cases from only one hospital, which was used to design and evaluate the proposed methods and adjust the hyper-parameters; (2) and the testing split with 40 cases from the four centers (10 cases per center) for the final testing and comparison with other existing methods. Furthermore, to adequately leverage the limited cases of the development split to explore new methods, we adopted 4-fold cross validation in the development stage. All results reported in this study were tested on our test set.

The main metric used was the dice coefficient between the predictions and ground-truth masks.

$$Dice = \frac{2|\boldsymbol{M} \cap \boldsymbol{G}|}{|\boldsymbol{M}| + |\boldsymbol{G}|},$$

where M denotes the predicted segmentation masks and G denotes the ground-truth masks. For each segmentation category (TL, FL, AO [aortic trunk, which is TL∪FL], and BR), we calculated the dice score of each case independently and then averaged them to obtain the final score of this category. Because the segmentation of TL and FL is the most important part of AD segmentation for diagnosis and repair planning, we mainly focused on the performance of TL and FL segmentation. The segmentation results of AO and BR were also reported for a comprehensive analysis. We also calculated the average boundary distance between the predictions and ground-truth masks to evaluate the segmentation performance of the methods from a boundary-based perspective.

Overview of ADSeg

In ADSeg, the first network is a classical U-Net, with the CT volume as the input, and outputs the predicted segmentation results. The second network is further equipped with flap attention modules and requires two inputs: (1) the CT volume concatenated with the output feature of the first U-Net and (2) the predicted flap segmentation result from the first U-Net. The input flap prediction is only used by the flap attention modules for sampling key voxels, as shown in Figures 3 and 4. Further, details regarding the proposed flap attention module are presented in the next subsection. The detailed structure of the U-Net equipped with flap attention is shown in Figure 3. It comprises an encoder with four basic blocks and a decoder with three blocks. Each basic block is composed of two 3 × 3 × 3 convolution layers (followed by a rectified linear unit [ReLU] and group normalization layer) and an optional flap attention module between them. Between the adjacent blocks in the encoder, a 2 × 2 × 2 max pooling operator was applied for down-sampling. Correspondingly, before each block in the decoder, the output feature maps of the previous block were first up-sampled twice in resolution and then concatenated with the corresponding encoder feature maps with the same resolution, to aggregate the more precise localization information. The channel numbers were also doubled or halved when the resolutions were halved or doubled, respectively. The detailed output resolutions and numbers of output channels are listed in Table 8.

Flap attention

As the divider between the TL and FL, the intimal flap is of great importance for the separation of the TL and FL. In contrast to previous AD segmentation methods[17–19] that only focused on the aortic lumen, we aimed to lead ADSeg to explicitly perceive the intimal flap of AD. In addition to TL, FL, and BR supervision, we generated the flap annotation automatically to supervise the first network, enabling it to predict the segmentation mask of the flaps. With the predicted flap masks from the first U-Net, the specifically designed flap attention modules in the second network enhance the features of the flaps, aggregate the information from the upper and lower portions of the aorta, and alleviate the interference caused by the curved shape of the aorta.

Flap prediction

Given the TL annotation M_{TL} and FL annotation M_{FL}, the flap annotation M_{flap} can be automatically generated using the morphological dilation operator:

$$M_{flap} = (M_{TL} \oplus E) \cap (M_{FL} \oplus E)$$

where $\oplus$ denotes the morphological dilation operator and E denotes the 3 × 3 × 3 cubic structural element. With the generated flap annotation as supervision, the U-Nets can be trained to predict the flap masks. Specifically, we added an additional output channel to the final convolution layer to predict the intimal flaps. Subsequently, the losses between the predicted flaps and generated flap annotations were calculated and back-propagated. Therefore, during inference, the U-Net predicts the flaps together with TL, FL, and BR. It should be noted that in ADSeg, the flap predictions generated by the first network are used only to provide a reference for sampling key voxels in the flap attention modules of the second network. The prediction of the intimal flap is an intermediate target, instead of the final target.

Flap attention module

The pipeline of the flap attention module is shown in Figure 4. As can be seen, a group of flap voxels is sampled from different slices, which then communicates with each other through the transformer encoder layer.

Specifically, with the flap voxels predicted by the first network, the voxels with the top-N highest confidences for each slice were chosen as the key flap voxels. These sampled key voxels were used by all flap attention modules in the second network. These $N \times L$ key voxels from all L slices are stacked and input to the standard transformer encoder layer, which mainly contains a

multi-head self-attention module followed by a multi-layer perceptron with two fully connected layers. The information encoded in these key voxels is fused and refined through the transformer encoder layer. Finally, these refined key flap voxels with richer semantics and contextual information are placed at their original positions, and the following convolution layers in the U-Net propagate the aggregated information from these key flap voxels to other adjacent voxels in a step-by-step manner. Therefore, long-distance feature aggregation along the curved aorta is naturally implemented using key flap voxels as messengers. In our experiments, we set N to 1 for the input features with the smallest resolution and doubled it for the cases of doubled resolution.

Data pre-processing and data augmentation

Before inputting the CT volumes to the network, several pre-processing operations were applied to reduce the computation cost and normalize the inputs. First, the volumes were down-sampled by a factor of 0.5 and the z axis length L was additionally resized to no more than 512. Subsequently, to crop the CT volume parts that do not contain the aorta, we extracted all the voxels within approximately -250 to 600 HU (including thrombus) and performed a $3 \times 3 \times 3$ cubic morphological opening operation on these voxels.[17] The x-y center of the maximum connected component can approximate the x-y center of the target aorta region. Therefore, a 128×128 aorta square region around the approximated x-y center with $L \leq 512$ slices can be extracted. Only voxels in this region participated in the segmentation process, and all other voxels were directly regarded as the background. Subsequently, we generated flap annotations with the TL and FL annotations, as depicted in the section "flap attention." To reduce the GPU memory cost, the extracted aorta volumes were further down-sampled to a fixed size of $240 \times 96 \times 96$ (z axis length (number of slices) × x axis length × y axis length). In practice, the volume size can be adjusted according to the available computational resources. Finally, the aorta voxels were standardized to establish a mean and standard deviation of 0 and 1, respectively.

During training, to enrich the training set and alleviate over-fitting, we further randomly jittered the aorta regions and rotated the volumes and labels by $[-10, 10]$ degrees around the z axis. To further introduce more randomness to the voxel selection process and improve the robustness to some slight segmentation errors of the first network, during training, the N key voxels for each slice were randomly selected from the top-$5N$ voxels with the highest confidence scores, instead of directly selecting the top-N voxels, as in the inference stage.

Training and testing procedures

To stabilize training, a pragmatic two-step training strategy was adopted for ADSeg. In the first training step, only the first U-Net and its output convolution layer were optimized to learn the segmentation masks of the flaps. The second network and its output convolution layer were not run or updated. In the second step, only the second network and its output convolution layer were trained to obtain the final model. With reliable flap masks and features generated by the first pre-trained U-Net as input, the second network can be trained more smoothly and effectively. Finally, during the testing procedure, only the outputs of the second network and its output convolution layer are regarded as the final predictions because the features captured by the flap attention network are finer.

SUPPLEMENTAL INFORMATION

Supplemental information can be found online at https://doi.org/10.1016/j.patter.2023.100727.

ACKNOWLEDGMENTS

We would like to thank Yun Feng from the Center for Biological Imaging (CBI), Institute of Biophysics, Chinese Academy of Science, for her help in analyzing the images. We are grateful for the financial assistance provided by the National Natural Science Foundation of China (NSFC; grant nos. 81873919 and 82102154), the Key Research and Development Projects of Hubei Province (grant no. 2020BAB022), Basic and Applied Basic Research Foundation of Guangdong Province (grant no. 2019A1515110727), and the China Postdoctoral Science Foundation (grant nos. 2021M691156 and 2021T140238).

AUTHOR CONTRIBUTIONS

D.X.: conceptualization, formal analysis, data curation, visualization, methodology, writing - original draft, writing - review & editing. J.Q.: conceptualization, methodology, writing - original draft. Y.W.: data curation, software, formal analysis. H.Z.: data curation, formal analysis. X.Z.: resources, formal analysis. J.Q.: data curation. X.M.: data curation. Y.R.: conceptualization. H.H.: resources, formal analysis. W.L.: conceptualization. F.Y.: investigation, resources. H.Z.: conceptualization, methodology, formal analysis, funding acquisition. X.W.: methodology, formal analysis, writing - review & editing, supervision. C.Z.: supervision, project administration, writing - review & editing, funding acquisition.

DECLARATION OF INTERESTS

The authors declare no competing interests.

Received: November 23, 2022
Revised: January 16, 2023
Accepted: March 14, 2023
Published: April 14, 2023

REFERENCES

1. Hagan, P.G., Nienaber, C.A., Isselbacher, E.M., Bruckman, D., Karavite, D.J., Russman, P.L., Evangelista, A., Fattori, R., Suzuki, T., Oh, J.K., et al. (2000). The international registry of acute aortic dissection (IRAD): new insights into an old disease. JAMA *283*, 897–903. https://doi.org/10.1001/jama.283.7.897.
2. Erbel, R., Aboyans, V., Boileau, C., Bossone, E., Bartolomeo, R.D., Eggebrecht, H., Evangelista, A., Falk, V., Frank, H., Gaemperli, O., et al. (2014). 2014 ESC Guidelines on the diagnosis and treatment of aortic diseases: document covering acute and chronic aortic diseases of the thoracic and abdominal aorta of the adult. The Task Force for the Diagnosis and Treatment of Aortic Diseases of the European Society of Cardiology (ESC). Eur. Heart J. *35*, 2873–2926. https://doi.org/10.1093/eurheartj/ehu281.
3. Nienaber, C.A., and Clough, R.E. (2015). Management of acute aortic dissection. Lancet *385*, 800–811. https://doi.org/10.1016/S0140-6736(14)61005-9.
4. Dake, M.D., Kato, N., Mitchell, R.S., Semba, C.P., Razavi, M.K., Shimono, T., Hirano, T., Takeda, K., Yada, I., and Miller, D.C. (1999). Endovascular stent-graft placement for the treatment of acute aortic dissection. N. Engl. J. Med. *340*, 1546–1552. https://doi.org/10.1056/NEJM199905203402004.
5. Khan, I.A., and Nair, C.K. (2002). Clinical, diagnostic, and management perspectives of aortic dissection. Chest *122*, 311–328. https://doi.org/10.1378/chest.122.1.311.
6. Erbel, R., Alfonso, F., Boileau, C., Dirsch, O., Eber, B., Haverich, A., Rakowski, H., Struyven, J., Radegran, K., Sechtem, U., et al. (2001). Diagnosis and management of aortic dissection. Eur. Heart J. *22*, 1642–1681. https://doi.org/10.1053/euhj.2001.2782.
7. Pape, L.A., Awais, M., Woznicki, E.M., Suzuki, T., Trimarchi, S., Evangelista, A., Myrmel, T., Larsen, M., Harris, K.M., Greason, K., et al. (2015). Presentation, diagnosis, and outcomes of acute aortic dissection: 17-year trends from the international registry of acute aortic dissection. J. Am. Coll. Cardiol. *66*, 350–358. https://doi.org/10.1016/j.jacc.2015.05.029.
8. Kamman, A.V., van Herwaarden, J.A., Orrico, M., Nauta, F.J.H., Heijmen, R.H., Moll, F.L., and Trimarchi, S. (2016). Standardized protocol to analyze computed tomography imaging of type B aortic dissections. J. Endovasc. Ther. *23*, 472–482. https://doi.org/10.1177/1526602816642591.
9. Trimarchi, S., Tolenaar, J.L., Jonker, F.H.W., Murray, B., Tsai, T.T., Eagle, K.A., Rampoldi, V., Verhagen, H.J.M., van Herwaarden, J.A., Moll, F.L., et al. (2013). Importance of false lumen thrombosis in type B aortic dissection prognosis. J. Thorac. Cardiovasc. Surg. *145*, S208–S212. https://doi.org/10.1016/j.jtcvs.2012.11.048.
10. Tsai, T.T., Evangelista, A., Nienaber, C.A., Myrmel, T., Meinhardt, G., Cooper, J.V., Smith, D.E., Suzuki, T., Fattori, R., Llovet, A., et al. (2007).

Partial thrombosis of the false lumen in patients with acute type B aortic dissection. N. Engl. J. Med. *357*, 349–359. https://doi.org/10.1056/NEJMoa063232.

11. Pepe, A., Li, J., Rolf-Pissarczyk, M., Gsaxner, C., Chen, X., Holzapfel, G.A., and Egger, J. (2020). Detection, segmentation, simulation and visualization of aortic dissections: a review. Med. Image Anal. *65*, 101773. https://doi.org/10.1016/j.media.2020.101773.
12. Morais, P., Vilaça, J.L., Queirós, S., Bourier, F., Deisenhofer, I., Tavares, J.M.R.S., and D'Hooge, J. (2017). A competitive strategy for atrial and aortic tract segmentation based on deformable models. Med. Image Anal. *42*, 102–116. https://doi.org/10.1016/j.media.2017.07.007.
13. Gu, Z., Cheng, J., Fu, H., Zhou, K., Hao, H., Zhao, Y., Zhang, T., Gao, S., and Liu, J. (2019). CE-net: context encoder network for 2D medical image segmentation. IEEE Trans. Med. Imaging *38*, 2281–2292. https://doi.org/10.1109/TMI.2019.2903562.
14. Fan, D.P., Zhou, T., Ji, G.P., Zhou, Y., Chen, G., Fu, H., Shen, J., and Shao, L. (2020). Inf-net: automatic COVID-19 lung infection segmentation from CT images. IEEE Trans. Med. Imaging *39*, 2626–2637. https://doi.org/10.1109/TMI.2020.2996645.
15. Zhao, H., Huang, J., Zhou, Q., Chen, N., Liu, L., Wang, X., Wang, T., Chen, L., Liu, C., Zheng, C., and Yang, F. (2022). Deep learning-based optical-resolution photoacoustic microscopy for in vivo 3D microvasculature imaging and segmentation. Adv. Intell. Syst. *4*, 2200004. 2022. https://doi.org/10.1002/aisy.202200004.
16. Cao, L., Shi, R., Ge, Y., Xing, L., Zuo, P., Jia, Y., Liu, J., He, Y., Wang, X., Luan, S., et al. (2019). Fully automatic segmentation of type B aortic dissection from CTA images enabled by deep learning. Eur. J. Radiol. *121*, 108713. https://doi.org/10.1016/j.ejrad.2019.108713.
17. Chen, D., Zhang, X., Mei, Y., Liao, F., Xu, H., Li, Z., Xiao, Q., Guo, W., Zhang, H., Yan, T., et al. (2021). Multi-stage learning for segmentation of aortic dissections using a prior aortic anatomy simplification. Med. Image Anal. *69*, 101931. https://doi.org/10.1016/j.media.2020.101931.
18. Hahn, L.D., Mistelbauer, G., Higashigaito, K., Koci, M., Willemink, M.J., Sailer, A.M., Fischbein, M., and Fleischmann, D. (2020). CT-Based true- and false-lumen segmentation in type B aortic dissection using machine learning. Radiol. Cardiothorac. Imaging *2*, e190179. https://doi.org/10.1148/ryct.2020190179.
19. Lyu, T., Yang, G., Zhao, X., Shu, H., Luo, L., Chen, D., Xiong, J., Yang, J., Li, S., Coatrieux, J.L., and Chen, Y. (2021). Dissected aorta segmentation using convolutional neural networks. Comput. Methods Programs Biomed. *211*, 106417. https://doi.org/10.1016/j.cmpb.2021.106417.
20. Wobben, L.D., Codari, M., Mistelbauer, G., Pepe, A., Higashigaito, K., Hahn, L.D., Mastrodicasa, D., Turner, V.L., Hinostroza, V., Baumler, K., et al. (2021). Deep learning-based 3D segmentation of true lumen, false lumen, and false lumen thrombosis in type-B aortic dissection. Annu. Int. Conf. IEEE Eng. Med. Biol. Soc. *2021*, 3912–3915. https://doi.org/10.1109/EMBC46164.2021.9631067.
21. Krissian, K., Carreira, J.M., Esclarin, J., and Maynar, M. (2014). Semi-automatic segmentation and detection of aorta dissection wall in MDCT angiography. Med. Image Anal. *18*, 83–102. https://doi.org/10.1016/j.media.2013.09.004.
22. Dotter, C.T., Roberts, D.J., and Steinberg, I. (1950). Aortic length: angiocardiographic measurements. Circulation *2*, 915–920. https://doi.org/10.1161/01.cir.2.6.915.
23. van Engelen, A., Silva Vieira, M., Rafiq, I., Cecelja, M., Schneider, T., de Bliek, H., Figueroa, C.A., Hussain, T., Botnar, R.M., and Alastruey, J. (2017). Aortic length measurements for pulse wave velocity calculation: manual 2D vs automated 3D centreline extraction. J. Cardiovasc. Magn. Reson. *19*, 32. https://doi.org/10.1186/s12968-017-0341-y.
24. Ronneberger, O., Fischer, P., and Brox, T. U-net: convolutional networks for biomedical image segmentation. Medical Image Computing and Computer-Assisted Intervention–MICCAI 2015: 18th International Conference, Munich, Germany, October 5-9, 2015, Proceedings, Part III 18 (pp. 234-241). Springer International Publishing. https://doi.org/10.1007/978-3-319-24574-4_28.
25. Wang, X., Girshick, R., Gupta, A., and He, K. (2018). Non-local neural networks. In Proceedings of the IEEE conference on computer vision and pattern recognition (IEEE), pp. 7794–7803. https://doi.org/10.48550/arXiv.1711.07971.
26. Huang, Z., Wang, X., Wei, Y., Huang, L., Shi, H., Liu, W., and Huang, T.S. (2020). CCNet: criss-cross attention for semantic segmentation. IEEE Trans. Pattern Anal. Mach. Intell. 1. https://doi.org/10.1109/TPAMI.2020.3007032.
27. Zhao, H., Shi, J., Qi, X., Wang, X., and Jia, J. (2017). Pyramid Scene Parsing Network, pp. 2881–2890. https://doi.org/10.48550/arXiv.1612.01105.
28. Cheng, T., Wang, X., Huang, L., and Liu, W. (2020). Boundary-preserving mask r-cnn. In Computer Vision–ECCV 2020: 16th European Conference, Glasgow, UK, August 23–28, 2020, Proceedings, Part XIV, *16*, pp. 660–676. https://doi.org/10.1007/978-3-030-58568-6_39.
29. Kirillov, A., Wu, Y., He, K., and Girshick, R. (2020). Pointrend: image segmentation as rendering. In Proceedings of the IEEE/CVF conference on computer vision and pattern recognition (IEEE), pp. 9799–9808. https://doi.org/10.48550/arXiv.1912.08193.
30. Ke, L., Danelljan, M., Li, X., Tai, Y.-W., Tang, C.-K., and Yu, F. (2022). Mask transfiner for high-quality instance segmentation. In Proceedings of the IEEE/CVF Conference on Computer Vision and Pattern Recognition (IEEE), pp. 4412–4421. https://doi.org/10.48550/arXiv.2111.13673.
31. Evangelista, A., Salas, A., Ribera, A., Ferreira-González, I., Cuellar, H., Pineda, V., González-Alujas, T., Bijnens, B., Permanyer-Miralda, G., and Garcia-Dorado, D. (2012). Long-term outcome of aortic dissection with patent false lumen: predictive role of entry tear size and location. Circulation *125*, 3133–3141. https://doi.org/10.1161/CIRCULATIONAHA.111.090266.
32. Wolterink, J.M., Leiner, T., de Vos, B.D., van Hamersvelt, R.W., Viergever, M.A., and Išgum, I. (2016). Automatic coronary artery calcium scoring in cardiac CT angiography using paired convolutional neural networks. Med. Image Anal. *34*, 123–136. https://doi.org/10.1016/j.media.2016.04.004.
33. Livne, M., Rieger, J., Aydin, O.U., Taha, A.A., Akay, E.M., Kossen, T., Sobesky, J., Kelleher, J.D., Hildebrand, K., Frey, D., and Madai, V.I. (2019). A U-net deep learning framework for high performance vessel segmentation in patients with cerebrovascular disease. Front. Neurosci. *13*, 97. https://doi.org/10.3389/fnins.2019.00097.
34. Zhao, H., Zhou, Z., Wu, F., Xiang, D., Zhao, H., Zhang, W., Li, L., Li, Z., Huang, J., Hu, H., et al. (2022). Self-supervised learning enables 3D digital subtraction angiography reconstruction from ultra-sparse 2D projection views: a multicenter study. Cell Rep. Med. *3*, 100775. https://doi.org/10.1016/j.xcrm.2022.100775.
35. Stroe, P., Claridge, E., and Odintsova, E. (2016). Cell boundary detection for quantitative studies of the role of tetraspanin CD82 in cell-cell adhesion. Procedia Comput. Sci. *90*, 107–112. https://doi.org/10.1016/j.procs.2016.07.031.
36. Paszke, A., Gross, S., Massa, F., Lerer, A., Bradbury, J., Chanan, G., Killeen, T., Lin, Z., Gimelshein, N., and Antiga, L. (2019). Pytorch: an imperative style, high-performance deep learning library. Adv. Neural Inf. Process. Syst. *32*. https://doi.org/10.48550/arXiv.1912.01703.
37. Kingma, D.P., and Ba, J. (2014). Adam: a method for stochastic optimization. Preprint at arXiv. https://doi.org/10.48550/arXiv.1412.6980.